# Effects of Salt on the Stability of a G-Quadruplex from the Human c-MYC Promoter

Byul G. Kim, Heather M. Evans, David N. Dubins, and Tigran V. Chalikian*

Department of Pharmaceutical Sciences, Leslie Dan Faculty of Pharmacy, University of Toronto, 144 College Street, Toronto, Ontario M5S 3M2, Canada

ABSTRACT: In an atmosphere of potassium ions, a modified c-MYC NHE III$_1$ sequence with two G-to-T mutations (MYC22-G14T/G23T) forms a highly stable parallel-stranded G-quadruplex. The G-quadruplex exhibits a steady increase in its melting temperature, T_M, with an increase in the concentration of the stabilizing cation K$^+$. On the other hand, an increase in the concentration of nonstabilizing Cs$^+$ or TMA$^+$ cations at a constant concentration of K$^+$ causes a sharp decline in T_M followed by a leveling off at ∼200 mM Cs$^+$ or TMA$^+$. At 51 °C and 600 μM K$^+$, an increase in Cs$^+$ concentration from 0 to 800 mM leads to a complete unfolding of the G-quadruplex. These observations are consistent with the picture in which more counterions accumulate in the vicinity of the unfolded state of MYC22-G14T/G23T (nonspecific ion binding) than in that of the G-quadruplex state. We estimate that the unfolded state condenses one extra counterion compared to the G-quadruplex state. Taken together with our earlier results, our data suggest that sodium or potassium cations sequestered inside the central cavity stabilize the G-quadruplex conformation acting as specifically bound ligands. Nonspecifically bound (condensed) counterions may slightly stabilize, exert no influence (human telomeric G-quadruplexes), or strongly destabilize (MYC22-G14T/G23T) the G-quadruplex conformation. We offer a structural rationalization for the enhanced thermal stability of the MYC22-G14T/G23T G-quadruplex.
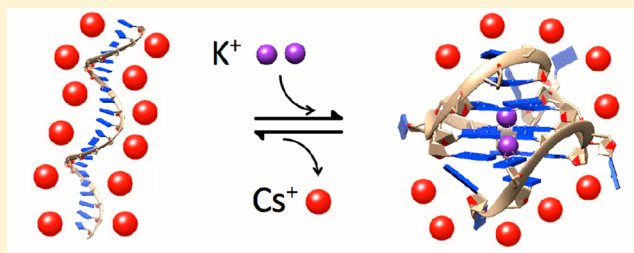
Guanine-rich single-stranded DNA stretches exhibit a propensity to spontaneously dissociate from their complementary strands and fold into various G-quadruplex structures in which guanine bases associate into plain hydrogen-bonded arrangements termed G-quartets.[1−3] In general, the G$_m$L$_1$G$_m$L$_2$G$_m$L$_3$G$_m$ sequence motifs (where m refers to the number of guanine repeats within the G-stretch and L$_1$−L$_3$ signify a nucleotide combination forming the loops between the respective G-stretches) may, under favorable conditions, form G-quadruplexes even with the complementary DNA strand present.[3−5] There is a growing body of evidence that DNA and RNA G-quadruplexes exist *in vivo* with ensuing biological implications.[6−9] Consensus G-quadruplex sequence motifs have been found in important loci of the genome, including telomeres, centromeres, immunoglobulin switch regions, mutation-prone hot spots, and promoter regions of oncogenes (such as *c-myc*, *c-myb*, *c-fos*, and *c-abl*).[2,5,10−13]

The c-MYC oncogene encodes a transcription factor that upregulates expression of many genes, thereby playing an important role in cell proliferation, growth, differentiation, angiogenesis, and apoptosis.[14−16] The aberrant overexpression of c-MYC is linked to the progression of a variety of human cancers, including colon, cervical, breast, prostate, and small-cell lung cancers, as well as osteosarcomas, leukemias, and lymphomas.[14,16,17] Roughly 90% of c-MYC transcriptional activation is controlled by highly conserved nuclease-hypersensitive element III$_1$ (NHE III$_1$), which is located 142−115 bp upstream from the P1 promoter of the oncogene.[17−20] NHE III$_1$ consists of the complementary coding pyrimidine-rich and noncoding purine-rich strands that, *in vitro*, can separately adopt the i-motif and G-quadruplex conformations, respectively.[18,21] Under conditions of transcriptionally induced negative superhelicity, the NHE III$_1$ domain exists in a slow equilibrium among the B-DNA double-stranded conformation, the single-stranded conformation, and a combination of the tetra-stranded i-motif (coding strand) and G-quadruplex (noncoding strand) conformations.[17,22,23] The G-quadruplex that forms within NHE III$_1$ acts as a silencer element in downregulation of c-MYC transcription.[17,24]

The 27-mer purine-rich strand of c-MYC NHE III$_1$ [5′-TGGGGAGGGTGGGGAGGGTGGGGAAGG-3′ (Pu27)] contains five consecutive runs of guanines. Both the I, II, III, and IV and II, III, IV, and V consecutive guanine runs have the ability to fold into G-quadruplexes. Nevertheless, in the single-stranded state of Pu27, the first run of guanines (G2−G5) is not involved in the formation of the physiologically relevant G-quadruplex. The II, III, IV, and V runs of guanines of NHE III$_1$ predominantly form the basis of its folding into the G-quadruplex-based silencer element.[24,25] However, when incorporated into a supercoiled plasmid and, consequently, within the context of duplex DNA under negative superhelicity,

the more stable G-quadruplex appears to involve the I, II, III, and IV guanine runs.[23]

Studies of the c-MYC NHE III$_1$ sequence as well as its *myc-1234* (5′-TGGGGAGGGTGGGGAGGGTGGGGA-3′) and *myc-2345* (5′-TGAGGGTGGGGAGGGTGGGGAA-3′) fragments and their modifications have established that, in the presence of K$^+$ ions, these sequences adopt the parallel G-quadruplex conformation with three double-chain-reversal loops bridging G-quartet layers.[25−28] The presence of the two four-guanine stretches in the *myc-1234* and *myc-2345* sequences gives rise to ambiguities with respect to the actual topology of the G-quadruplexes. Introduction of two G-to-T mutations at residue positions 14 and 23 of the original c-MYC (Pu 27) sequence (5′-TGAGGGTGGGTAGGGTGGGTAA-3′) restricts the modified sequence (MYC22-G14T/G23T) to adopting a single, parallel-stranded G-quadruplex conformation.[27] The conformational singularity renders the MYC22-G14T/G23T sequence an attractive candidate for thermodynamic investigations, affording a more straightforward interpretation of resulting data while also being biologically important. In general, K$^+$-stabilized G-quadruplex structures are viewed as being more biologically relevant than the Na$^+$-stabilized structures given the higher concentration of potassium ions inside the cell.

Identification and thermodynamic characterization of the forces that stabilize or destabilize G-quadruplex conformations of guanine-rich strands relative to their double- and single-stranded conformers are fundamentally and practically important.[3,29] In particular, they are important for elucidating mechanisms of biological control of G-quadruplex-based genetic switches and devising ways for operational intervention in the induction and/or prevention of G-quadruplex formation at desired loci of the genome.

The polyanionic nature of the DNA and the resulting high charge density give rise to the accumulation of ions around the DNA caused by the Debye−Hückel screening and counterion condensation.[30−34] Given the entropic forces originating from the "polyelectrolyte effect", an increase in the solution ionic strength shifts the equilibrium between nucleic acid species toward the conformer at which more counterions accumulate.[30−34] For example, an increase in the salt concentration shifts the equilibrium between the helix and coil states of polymeric nucleic acid duplexes and T-rich triplexes toward the helical conformation in which more counterions accumulate.[35,36]

The polyelectrolyte effect is weakened in oligomeric nucleic acids because of the lower charge density around the ends of a duplex (the Coulombic end effects).[37] The weakening is demonstrated, in particular, in some reduction in the salt dependence of the melting temperature, T_M, of oligomeric relative to polymeric DNA duplexes.[36−39] Understandably, the relative contribution of Coulombic end effects decreases as the DNA becomes longer. Double-stranded oligomeric DNA helices with ≥15 nucleotides display slopes $(\partial T_M/\partial \ln[\text{salt}])$ that differ by <10% from those displayed by polymeric DNA.[37] Hence, the accumulation of ions around the 22-mer DNA studied in this work is significant, while the DNA can be analyzed as a polyelectrolyte.

The thermal stability (T_M) of G-quadruplexes, generally, increases with an increase in the concentration of the stabilizing ion.[3] However, compared to the case for duplexes and triplexes, the situation with G-quadruplexes is more subtle and interesting. Unlike other nucleic acid structures, G-quad-

ruplexes display specific ion binding inside the central cavity in addition to counterion condensation (nonspecific binding). Consequently, the observed increase in T_M may originate from both the specific and nonspecific ion binding events. In a previous publication, we have developed an experimental approach that allows one to separate the specific and nonspecific contributions to the salt-induced increase in G-quadruplex stability.[40] The melting temperature, T_M, of a G-quadruplex preformed at saturating concentrations of the stabilizing ion is separately measured as a function of the concentration of stabilizing and nonstabilizing [such as Cs$^+$ or tetramethylammonium (TMA$^+$) ion] monovalent cations.[40] A change in T_M upon addition of the stabilizing cation (Na$^+$ or K$^+$) is governed by a combination of specific (internal binding) and nonspecific (counterion condensation) salt effects. In contrast, a change in T_M accompanying the addition of a nonstabilizing cation is solely due to nonspecific binding. Hence, the differential response of T_M to a change in the concentration of the stabilizing and nonstabilizing cations can be used to discriminate between the effects of specific and nonspecific ion binding.

With this approach, we have studied two G-quadruplexes formed by human telomeric sequences that are distinct with respect to their folding topologies and the identity and number of sequestered stabilizing ions (Na$^+$-stabilized antiparallel and K$^+$-stabilized hybrid structures).[40] Our data are consistent with the picture in which the electrostatic contribution to G-quadruplex stability is overwhelmingly due to the specifically bound Na$^+$ or K$^+$ ions.[40] Counterion condensation has little to no stabilizing influence.[40]

In this work, we expand our studies to characterizing the K$^+$-stabilized parallel G-quadruplex formed by the MYC22-G14T/G23T sequence. As mentioned above, MYC22-G14T/G23T is an attractive subject of thermodynamic investigations given its biological relevance and singularity of structure. Another peculiarity of the MYC22-G14T/G23T G-quadruplex is its high thermal stability and the ability to form a G-quadruplex at extremely low K$^+$ concentrations.[27,41] Our results indicate a strongly destabilizing influence of the polyelectrolyte effect on the G-quadruplex formed by the MYC22-G14T/G23T sequence. We also find that the MYC22-G14T/G23T G-quadruplex can be unfolded by an increase in the concentration of the nonstabilizing counterion cesium. This is a remarkable result that, to the best of our knowledge, has never been reported for other nucleic acid structures.

■ MATERIALS AND METHODS

Materials. The MYC22-G14T/G23T oligonucleotide (ODN) sequence 5′-TGAGGGTGGGTAGGGTGGGTAA-3′ was purchased from two sources, ACGT, Inc. (Toronto, ON), and Integrated DNA Technologies (Coralville, IA). We did not observe any statistically significant differences in our experimental results obtained with the ACGT or IDT DNA samples. Potassium chloride, cesium chloride, tetramethylammonium chloride, tetrabutylammonium hydroxide, and phosphoric acid were obtained from Sigma-Aldrich Canada (Oakville, ON). EDTA (free acid) was purchased from Fisher Biotech (Fair Lawn, NJ). All reagents were of the highest commercially available grade and used without further purification. The solutions were prepared using doubly distilled water.

The ODN was initially dissolved in and dialyzed against a buffer consisting of 10 mM phosphoric acid titrated to pH 7.0 with tetrabutylammonium hydroxide, 0.1 mM EDTA, and the

desired levels of KCl, CsCl, or TMACl. Dialysis was performed in 1000 Da molecular mass cutoff Tube-O-Dialyzers from G Biosciences (St. Louis, MO). In the absence of any added salt, the tetrabutylammonium phosphate buffer does not support the folded G-quadruplex conformation of the ODN. Given their large size, tetrabutylammonium (TBA^+) ions are fully excluded from the central cavity of the G-quadruplex and, therefore, cannot stabilize a G-quadruplex.

The concentrations of the oligonucleotide were determined from the UV light absorbance at 260 nm measured at 25 °C with a Cary 300 Bio spectrophotometer (Varian Canada, Inc., Mississauga, ON) using a molar extinction coefficient of 228700 M^{-1} cm^{-1} for the unfolded conformation. The latter was calculated using an additive nearest neighbor procedure as described by R. Owczarzy (http://www.owczarzy.net/extinct. htm). In our CD measurements and temperature-dependent UV light absorption measurements, the ODN concentration was adjusted to ~30 and ~3 μM, respectively.

Circular Dichroism (CD) Spectroscopy. The CD spectra of the ODN were recorded in a 1 mm path-length cuvette using an Aviv model 62 DS spectropolarimeter (Aviv Associates, Lakewood, NJ). CD spectroscopic measurements were used to probe the conformations adopted by the ODN under various experimental conditions employed in this study.

UV Melting Experiments. UV light absorption at 295 nm was measured as a function of temperature in ODN samples contained in a 1 cm path-length cuvette. The measurements were performed with a Cary 300 Bio spectrophotometer (Varian Canada, Inc.). The temperature was changed at a rate of 1 °C/min. The G-quadruplex-to-coil transition temperatures, T_M, and van't Hoff enthalpies, ΔH_{vH}, were evaluated from our experimental UV melting profiles using the standard procedures.[42,43]

Computation of Solvent Accessible Surface Areas and Molecular Volumes. Our analysis was based on the NMR-determined potassium-induced G-quadruplex structure of MYC22-G14T/G23T (Protein Data Bank entry 1XAV) obtained from the RCSB Protein Data Bank. We calculated the solvent accessible surface area, S_A, for the G-quadruplex as the sum of the accessible surface areas of all atoms in the structure. The intrinsic volume, V_M, of the ODN was calculated as molecular volumes as described by Richards.[44,45] MSP (Molecular Surface Package) version 3.9.3 was obtained from M. Connolly at www.biohedron.com and used to calculate the solvent accessible surface area and molecular volume, using a 1.4 Å probe radius on a Linux platform.

RESULTS

K^+-Induced G-Quadruplex Formation. Figure 1a presents the CD spectra of MYC22-G14T/G23T in a 10 mM TBA-phosphate buffer at various K^+ concentrations. Inspection of Figure 1a reveals that MYC22-G14T/G23T undergoes a K^+-induced transition to a G-quadruplex conformation. The CD spectrum of the G-quadruplex presented in Figure 1a is consistent with that reported by Hatzakis et al.[46] for the same sequence. It exhibits a positive maximum at 264 nm and a negative minimum at 244 nm, features characteristic of the parallel structure with three double-chain-reversal loops bridging the G-quartets.[47] This notion is consistent with the NMR-derived structure of the K^+-stabilized MYC22-G14T/G23T G-quadruplex.[27] Note that the isoelliptic point observed at 254 nm is suggestive of the two-stateness of the K^+-induced folding transition.
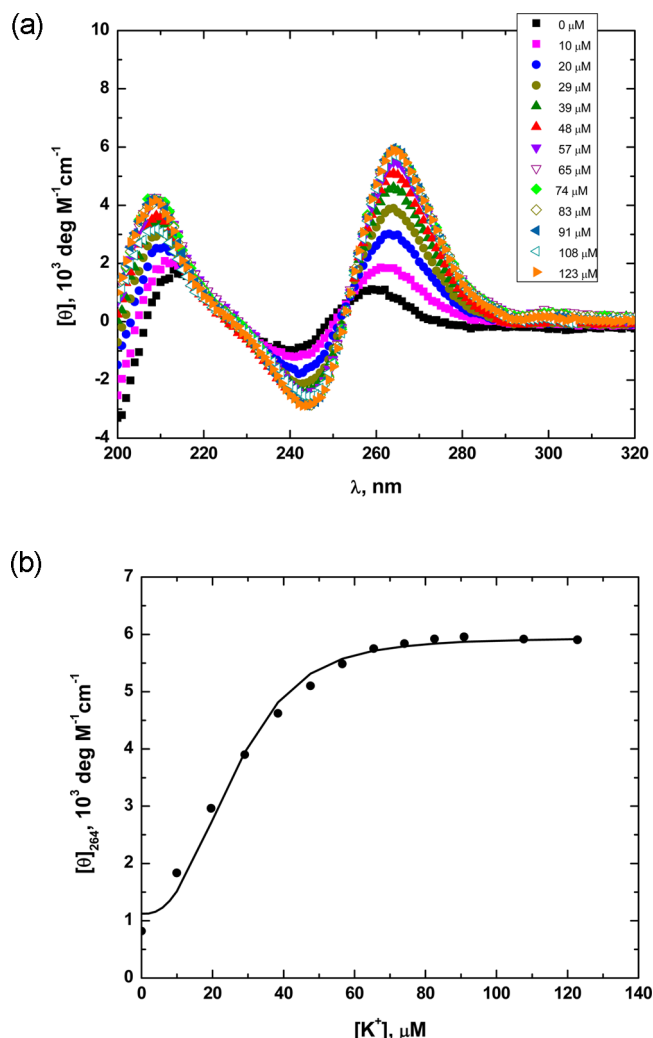

Figure 1. (a) CD spectra of MYC22-G14T/G23T in a 10 mM TBA-phosphate buffer at various KCl concentrations at 25 °C. (b) Dependence of the molar ellipticity of MYC22-G14T/G23T at 264 nm on the KCl concentration. Experimental data were approximated with eq 2 for $n = 3$ (—).

Figure 1b shows the K^+ dependence of the molar ellipticity of MYC22-G14T/G23T at 264 nm. Inspection of Figure 1b reveals that G-quadruplex formation is complete at ~80 μM K^+. Given the ODN concentration of ~35 μM, this observation suggests an extremely tight apparent binding of potassium ions to MYC22-G14T/G23T with its subsequent folding into a G-quadruplex. For comparison, human telomeric sequences form G-quadruplexes at Na^+ or K^+ concentrations of 10−20 mM.[48,49]

We used UV absorption at 295 nm to monitor the heat-induced G-quadruplex unfolding transitions at 100, 300, 600, 1000, and 3000 μM KCl.[50] Figure 2a shows a representative UV melting profile of MYC22-G14T/G23T at 1 mM KCl. The melting profiles were approximated by the two-state transition model from which the melting temperatures, T_M, and van't Hoff enthalpies, ΔH_{vH}, were determined.[42,43,51] It should be noted, however, that heat-induced G-quadruplex melting transitions are, generally, not two-state and may involve one or more intermediates between the folded and unfolded states.[52]

In strict terms, if intermediates are present, a single T_M becomes physically unsound. More rigorous alternatives may be
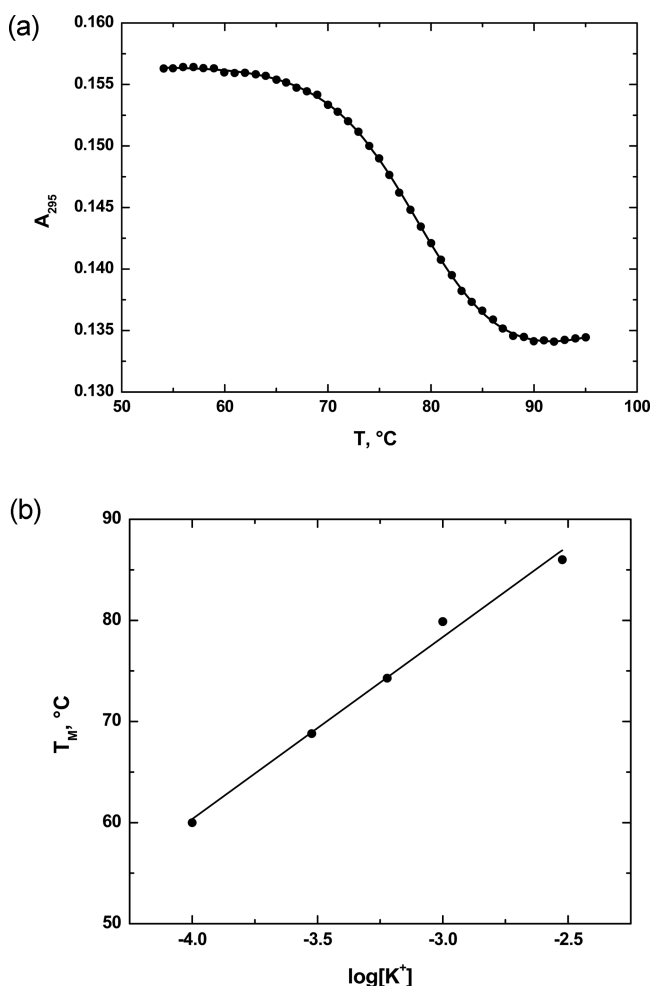
(a)

(b)

Figure 2. (a) Representative UV melting profile at 295 nm of the MYC22-G14T/G23T G-quadruplex at 1 mM KCl. (b) Dependence of the melting temperature, T_M, of the MYC22-G14T/G23T G-quadruplex on the concentration of K^+ ions. Experimental data were approximated by an exponential function solely to guide the eye (—).

the temperatures at which 50% of the DNA is folded, T_F, or fully unfolded, T_U. Determination of T_F and T_U is experimentally demanding and, generally, cannot be accomplished on the basis of a single UV melting profile. As a reasonable approximation, the T_M operationally defined as the transition midpoint can be equated with $\sim(T_F + T_U)/2$. In this respect, T_M is a useful and convenient qualitative measure of G-quadruplex stability. Moreover, if the width of the transition does not change significantly, a shift in T_M accompanying an alteration in solution conditions (e.g., ionic strength or solvent composition), ΔT_M, is roughly equal to $\Delta T_F \approx \Delta T_U$. Should the width of the transition change, the deviation of ΔT_M from ΔT_F and ΔT_U should be on the same order of magnitude as the change in the transition width. Hence, ΔT_M is a robust measure of the G-quadruplex stability response to a change in environmental conditions.

On the other hand, the model-dependent van't Hoff enthalpy, ΔH_{vH}, determined from UV melting profiles may significantly differ from the true transition enthalpy. The latter can be determined on the basis of differential scanning calorimetric (DSC) measurements.[53,54] In addition, the transition enthalpy may depend on temperature. This possibility is underscored by non-zero changes in heat capacity,

ΔC_p, suggested for G-quadruplex melting transitions.[55] Given the uncertainty related to the ΔH_{vH} values, we limit their use to estimating the differential number of counterions, Δn_{M^+}, released to or taken up from the bulk upon the G-quadruplex-to-coil transitions. We treat the determined values of Δn_{M^+} as qualitative rather than quantitative estimates.

Figure 2b plots the transition temperatures, T_M, of the MYC22-G14T/G23T G-quadruplex against the K^+ concentration. In agreement with a previous report, the MYC22-G14T/G23T G-quadruplex exhibits an unusually high thermal stability.[27] For example, at 1 mM KCl, the T_M is 79.9 ± 0.2 °C. For comparison, the melting temperature of the K^+-stabilized hybrid-1 G-quadruplex formed by the 26-mer human telomeric sequence $d[A_3G_3(T_2AG_3)_3A_2]$ is 70.6 ± 0.3 °C at 200 mM KCl.[49]

The values of T_M shown in Figure 2b are significantly higher than similar data measured by Hatzakis et al. for the MYC22-G14T/G23T sequence.[46] These authors report melting temperatures, T_M, of 43, 57, 64, 69, 75, and 80 °C at K^+ concentrations of 0.5, 2, 5, 10, 20, and 50 mM, respectively.[46] For comparison, we measured T_M values of 60.0 ± 0.2, 68.8 ± 0.2, 74.3 ± 0.2, 79.9 ± 0.2, and 86.0 ± 0.3 °C at 0.1, 0.3, 0.6, 1, and 3 mM KCl, respectively (see Figure 2b). At higher K^+ concentrations, the melting points of the MYC22-G14T/G23T G-quadruplex approached and exceeded 100 °C and, therefore, were beyond the experimentally attainable temperature range. As explained above, we conducted our measurements on DNA samples obtained from two independent commercial sources. Our spectrophotometrically determined values of T_M were in excellent agreement with the results of our circular dichroism and differential scanning calorimetric measurements (data not shown). Currently, we do not have a viable explanation for the discrepancy between our results and those of Hatzakis et al.[46] It should be noted, however, that our measurements were conducted in the presence of 10 mM TBA phosphate buffer, while Hatzakis et al. used a 10 mM lithium phosphate buffer.[46] Further studies are required to explore the possibility of the buffer playing a role in the observed discrepancies in T_M.

Conformational Preferences of the K^+-Stabilized G-Quadruplex with Large Excesses of Cs^+ and TMA^+ Ions. Because of their size, Cs^+ and TMA^+ ions do not fit inside the central cavity of a G-quadruplex. If added to a preformed G-quadruplex, Cs^+ and TMA^+ ions will influence the G-quadruplex stability through the polyelectrolyte effect. Figure 3a shows the CD spectra of the MYC22-G14T/G23T G-quadruplex recorded in 300 μM KCl to which CsCl was incrementally added to a final concentration of 800 mM. Inspection of Figure 3a reveals that Cs^+ does not cause noticeable structural changes in the MYC22-G14T/G23T G-quadruplex. Similar observations were made at 600 and 1000 μM KCl (data not shown).

To ensure the lack of kinetically trapped conformations of MYC22-G14T/G23T, the CD spectra of the G-quadruplex in 300 μM KCl to which 800 mM CsCl was subsequently added were recorded as the temperature was incrementally increased from 25 to 80 °C (above unfolding) and then decreased to 25 °C. Figure 3b presents the CD spectra at increasing (25, 40, 60, and 80 °C) and decreasing (60, 40, and 25 °C) temperatures. At 25 °C, the original CD spectrum coincides with that of the annealed G-quadruplex, an observation that excludes the existence of kinetically trapped states. However, if CsCl was added prior to KCl, the ODN adopts, at least partially, a kinetically trapped state(s). One arrives at this conclusion on
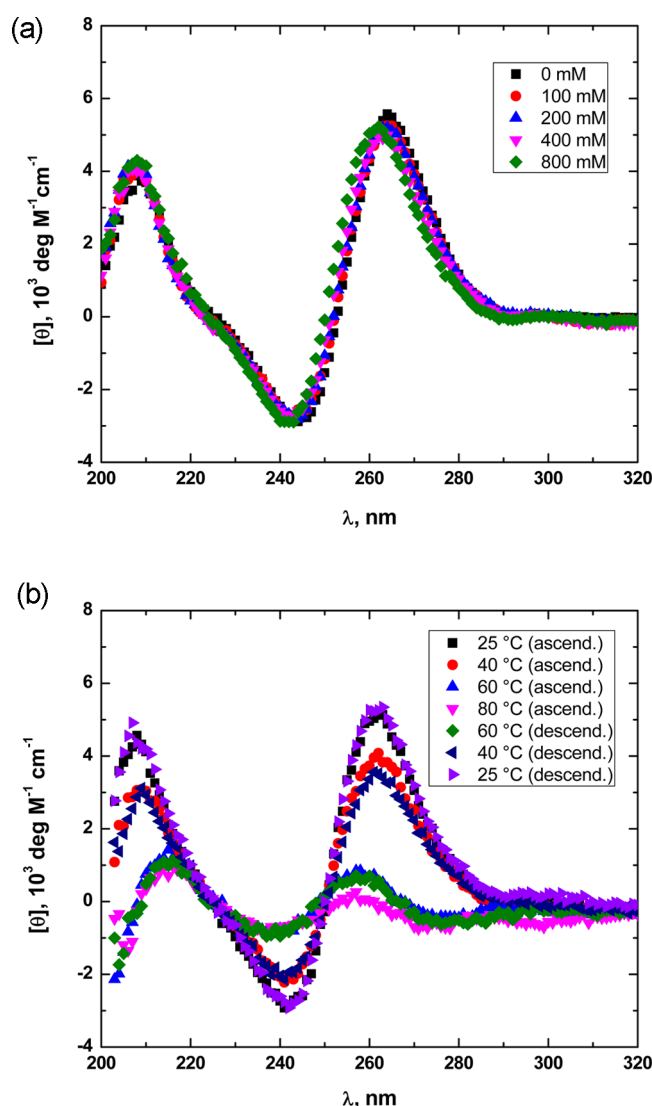
(a)

(b)

Figure 3. (a) CD spectra of the MYC22-G14T/G23T G-quadruplex at 300 μM KCl at various CsCl concentrations. (b) CD spectra of the MYC22-G14T/G23T G-quadruplex preformed in 300 μM KCl with 800 mM CsCl added subsequently at temperatures increasing from 25 to 80 °C and decreasing to 25 °C.

(a)

(b)

Figure 4. (a) CD spectra of the MYC22-G14T/G23T G-quadruplex at 300 μM KCl at various TMACl concentrations. (b) CD spectra of the MYC22-G14T/G23T G-quadruplex preformed in 300 μM KCl with 800 mM TMACl added subsequently at temperatures increasing from 25 to 80 °C and decreasing to 25 °C.

the basis of an ∼20% increase in the intensity of the CD band at 265 nm of the annealed relative to the initial ODN at 25 °C (data not shown).

Figure 4a shows the CD spectra of the G-quadruplex preformed in 300 μM KCl with TMACl subsequently added in increments to concentrations of up to 800 mM. Analogous to CsCl, no TMA⁺-induced changes in the conformation of the K⁺-stabilized MYC22-G14T/G23T G-quadruplex can be observed. No TMA⁺-induced CD spectral changes were observed at 600 and 1000 μM KCl (data not shown).

Figure 4b presents the CD spectra of the G-quadruplex preformed in the presence of 300 μM KCl, to which 800 mM TMACl was subsequently added, as the temperature was increased in a stepwise manner from 25 to 80 °C and then decreased to 25 °C. The CD spectra of the initial and annealed ODN at 25 °C are identical, which suggests the absence of kinetically trapped states. However, if TMACl was added prior to KCl, the ODN adopts a kinetically trapped state(s). This inference can be drawn on the basis of an ∼20% increase in the
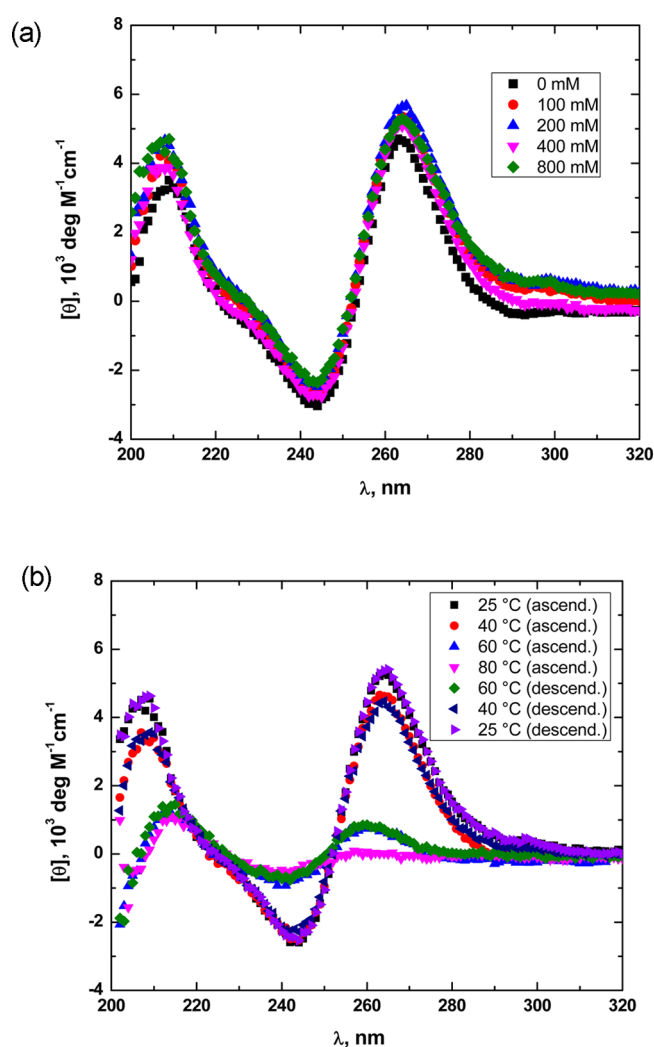
intensity of the CD band at 265 nm when the sample is heated to 80 °C and then cooled to 25 °C (data not shown).

Thermal Stability of the K⁺-Stabilized G-Quadruplex in the Presence of Cs⁺ and TMA⁺ Ions. Panels a−c of Figure 5 show the Cs⁺ dependencies of the melting temperatures, T_M, for the G-quadruplex preformed at 300, 600, and 1000 μM KCl, respectively. Inspection of Figure 5 reveals that, for all KCl concentrations, the T_M steeply decreases as the Cs⁺ concentration increases from 0 to ∼200 mM and levels off at higher concentrations.

Panels a−c of Figure 6 present the TMA⁺ dependencies of the melting temperatures, T_M, for the MYC22-G14T/G23T G-quadruplex preformed at 300, 600, and 1000 μM KCl, respectively. Analogous to the case for CsCl, the addition of TMACl causes a steep decrease in T_M between 0 and ∼200 mM TMA⁺ followed by a plateau at higher concentrations.

Given the diminution in the stability of the MYC22-G14T/G23T G-quadruplex under the influence of Cs⁺ and TMA⁺ ions, it can be anticipated that, at some temperatures, the G-quadruplex-to-coil transition can be triggered by addition of nonstabilizing cations, such as Cs⁺ or TMA⁺. To test this
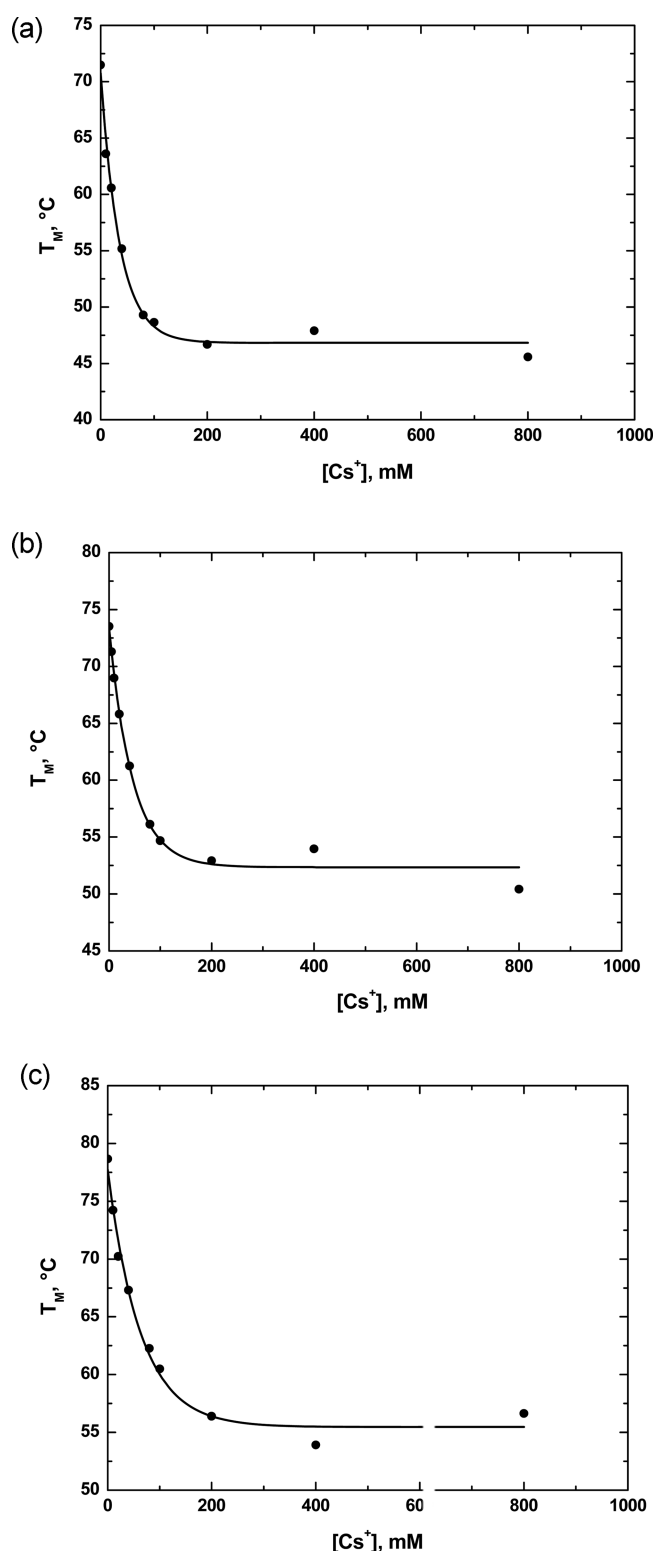
Figure 5. Dependencies of the melting temperature, T_M, of the MYC22-G14T/G23T G-quadruplex on the concentration of CsCl at (a) 300, (b) 600, and (c) 1000 μM KCl. Experimental data were approximated by an exponential function solely to guide the eye (—).

Figure 6. Dependencies of the melting temperature, T_M, of the MYC22-G14T/G23T G-quadruplex on the concentration of TMACl at (a) 300, (b) 600, and (c) 1000 μM KCl. Experimental data were approximated by an exponential function solely to guide the eye (—).

hypothesis, we performed Cs$^+$-dependent CD spectral measurements at 51 °C and a representative K$^+$ concentration of 600 μM. At 51 °C without CsCl, MYC22-G14T/G23T predominantly exists in its G-quadruplex conformation. Addition of CsCl causes unfolding of the G-quadruplex as is seen from
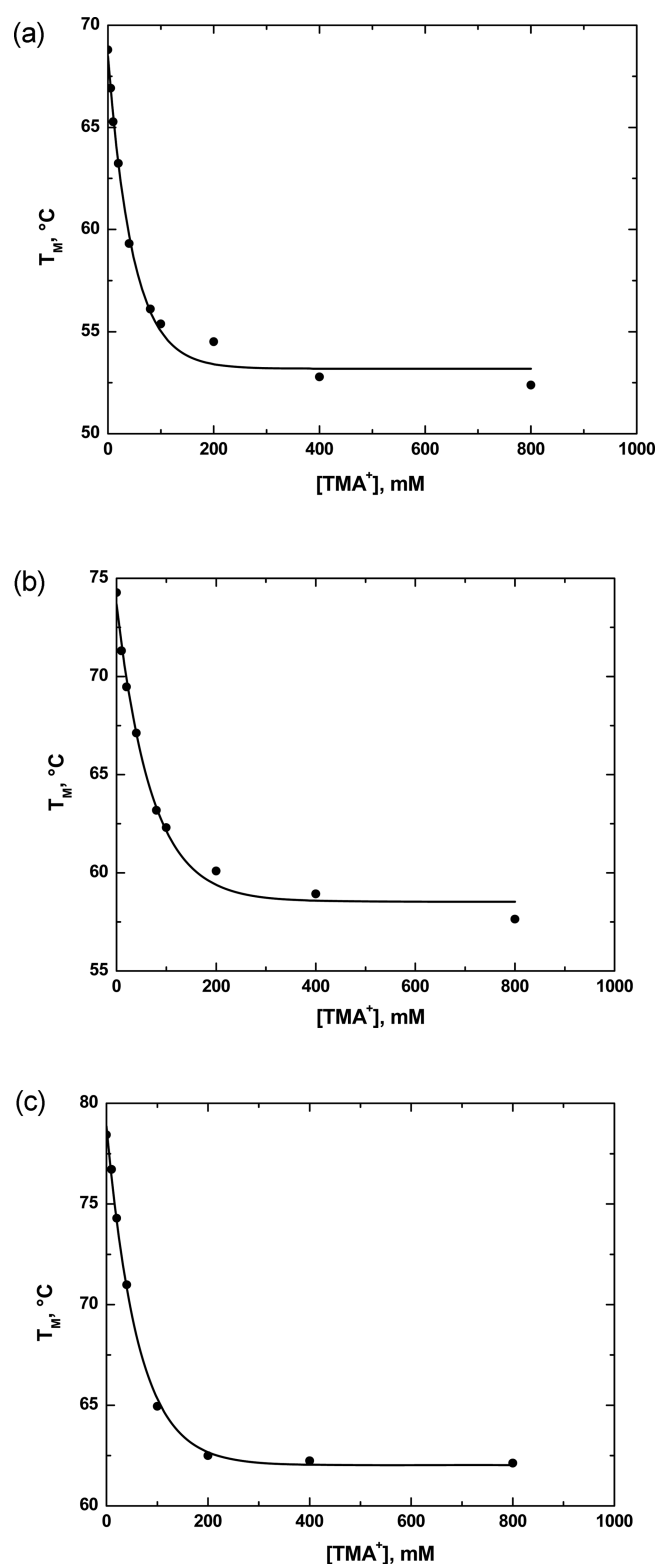
Figure 7. Inspection of Figure 7 reveals that MYC22-G14T/ G23T undergoes a sigmoidal G-quadruplex-to-coil transition with a midpoint at ~75 mM CsCl.
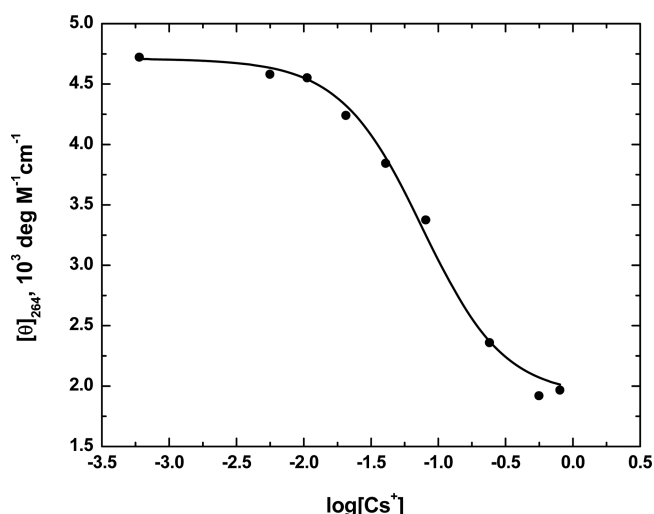
Figure 7. CsCl dependence of the molar ellipticity of MYC22-G14T/G23T at 264 nm in 600 μM KCl at 51 °C. Experimental data were approximated with eq 4 (—).

■ DISCUSSION

Stability of the MYC22-G14T/G23T G-Quadruplex. The apparent affinity of K$^+$ ions for the ODN is very high. As is seen from Figure 1b, G-quadruplex formation is nearly complete at a stoichiometric ratio of ~2 K$^+$ ions per ODN, which corresponds to the structural number of K$^+$ ions sequestered inside the central cavity of the G-quadruplex.[27] The K$^+$-induced coil (C)-to-G-quadruplex (Q) transition can be formally presented as the binding reaction:

$$C + nK^+ \leftrightarrow Q \qquad (1)$$
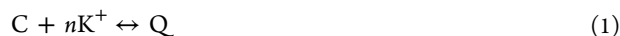
If a two-state transition is assumed, the apparent equilibrium constant of reaction 1 can be expressed as follows:

$$K_b = [Q]/([C][K^+]^n)$$
$$= \alpha/[(1 - \alpha)([K^+]_T - \alpha n[DNA])^n] \qquad (2)$$

where $[K^+]_T$ is the total concentration of potassium ions in solution, $[DNA] = [C] + [Q]$ is the total concentration of the ODN, $[K^+]$ is the concentration of unbound potassium ions, $\alpha = [Q]/[DNA]$ is the fraction of the ODN in the G-quadruplex conformation, and, consequently, $1 - \alpha = [C]/[DNA]$ is the fraction of the ODN in the coil conformation.

The fraction α can be evaluated for each experimental point of the titration profile presented in Figure 1b as the ratio $\alpha = \Delta X/\Delta X_{max}$, where ΔX is the change in an experimental observable (here, the molar ellipticity at 264 nm) relative to its initial value without K$^+$ and ΔX_{max} is the asymptotic maximum of ΔX corresponding to the fully folded state of the ODN. We fitted the titration profile presented in Figure 1b with eq 2 with n values of 1, 2, and 3. The fitting was performed numerically on the basis of a direct search optimization technique for fitting nonlinear systems.[56] The best fit of the data was achieved when n equaled 3 with an apparent equilibrium constant K_b of 1.19 × 10^{14} M^{-3}.

With n equal to 3, one can hypothesize that, in addition to the two NMR-detected potassium ions sequestered inside the central cavity,[27] there is an additional K$^+$ ion bound to the G-structure, albeit in a nonlocalized and/or unimmobilized (and, therefore, invisible to NMR) manner. A note of caution is warranted here. Although the isoelliptic point at 254 nm in

Figure 1a is consistent with two-stateness of the K$^+$-induced MYC22-G14T/G23T folding, folding—unfolding transitions of G-quadruplexes may not be two-state.[52,57] Consequently, we do not exclude the possibility that the best fit obtained at $n = 3$ may be an artifact related to the two-state approximation used to derive eq 2. At present, we view the resulting value of $n = 3$ as a qualitative (although realistic) estimate, which calls for further studies to determine the nature of the K$^+$-induced transition of MYC22-G14T/G23T and the number of associated potassium ions.

The K$^+$ dependence of the melting temperature, T_M, presented in Figure 2b can be used to evaluate the number of counterions released to the bulk upon the helix-to-coil transitions of the G-quadruplex:[31,58−60]

$$\Delta n_{M^+} = (\partial T_M/\partial \ln[M^+])\Delta H_M/RT_M^2 \qquad (3)$$

where Δn_{M^+} is differential number of counterions (M$^+$) thermodynamically associated with the ODN in the G-quadruplex and coil states.

The value of Δn_{M^+} in eq 3 equals a change in the combined preferential interaction parameter $[\Delta\Gamma = N\Delta i$, where N is the number of formal charges (phosphates) in the oligonucleotide and Δi is the difference in the thermodynamic degree of dissociation between the coil and G-quadruplex states].[32,33,58] It should be noted that n in reaction 1 does not, generally, coincide with Δn_{M^+} in eq 3. While n in reaction 1 refers to the specifically bound cations, Δn_{M^+} in eq 3 includes in addition the differential number of counterions that accumulated in the vicinity of the polyanionic ODN in its folded and unfolded states.

Application of eq 3 to Figure 2b yields a Δn_{M^+} of 1.8 ± 0.2, which is close to 2, the number of centrally bound potassium ions. At the quantitative level, the veracity of this result may be compromised by the use in eq 3 of the model-dependent van't Hoff enthalpy, ΔH_{vH}, instead of the true transition enthalpy, ΔH_{cal} (that can be measured by DSC). To assess the extent of the error, one can assume that, depending on the nature of the transition, the $\Delta H_{vH}/\Delta H_{cal}$ ratio may vary between the two extremes of 0.5 and 2. Within this limit, we estimate that Δn_{M^+} may range between 1 and 4. Thus, the use of the van't Hoff enthalpy in our calculations does not lead to a qualitative change in our estimates. Hence, realistically, our aggregate results emerging from Figures 1b and 2b suggest that the folding of MYC22-G14T/G23T is accompanied by an uptake of ~2 to ~3 potassium ions, in good agreement with structural data.

Cs$^+$ and TMA$^+$ Ions Do Not Cause Structural Alterations in the Preformed G-Quadruplex. Once formed in the atmosphere of K$^+$ ions, the MYC22-G14T/G23T G-quadruplex retains its conformation even at a large excess of Cs$^+$ or TMA$^+$ ions (see Figures 3a and 4a). The G-quadruplex conformation corresponds to the global minimum of the free energy. This notion follows from the observation that an annealing of the preformed G-quadruplex to which CsCl or TMACl was subsequently added does not result in CD spectral changes (see Figures 3b and 4b).

If, on the other hand, KCl is added to the ODN initially in 800 mM CsCl or TMACl, a kinetically trapped state(s) is formed. The kinetically trapped state(s) converts into the thermodynamically stable one once the solution is heated to 80 °C and then cooled to 25 °C.

In the UV melting experiments discussed below, the G-quadruplexes were preformed in KCl with the desired amounts

Table 1. Numbers of Formal Charges (N_q), Molecular Volumes (V_M), Solvent Accessible Surface Areas (S_A), and Volume (ρ_q) and Surface (σ_q) Charge Densities Computed for the c-MYC and Human Telomeric Tel22 and Tel26 G-Quadruplexes as Well as "an Average" Polymeric Duplex[a]

	N_q	V_M (Å^3)	S_A (Å^2)	ρ_q (×10^{-3} e/Å^3)	σ_q (×10^{-3} e/Å^2)
c-MYC	20	6178 ± 16	4442 ± 33	3.24 ± 0.01	4.50 ± 0.03
	(281 ± 1)	(202 ± 2)			
Tel22[b]	19	6426 ± 26	3907 ± 99	2.96 ± 0.01	4.9 ± 0.1
	(292 ± 1)	(178 ± 5)			
Tel26[c]	24	7092 ± 27	3963 ± 69	3.38 ± 0.01	6.1 ± 0.1
	(273 ± 1)	(152 ± 3)			
polymeric duplexes (per nucleotide)[d]	1	281 ± 8	162 ± 10	3.6 ± 0.1	6.2 ± 0.3

[a]The values of V_M and S_A normalized per nucleotide are shown in parentheses. [b]From ref 48. [c]From ref 49. [d]From ref 68.

of CsCl or TMACl added afterward. In addition, the ODN samples were annealed prior to experiments. Therefore, when interpreting our data, we assume that the ODN exists in a single, thermodynamically stable G-quadruplex conformation.

Modulation of G-Quadruplex Stability by Cs$^+$ and TMA$^+$ Ions. At every KCl concentration studied, the thermal stability, T_M, of the G-quadruplex sharply decreases as the concentration of Cs$^+$ or TMA$^+$ ions increases and levels off above ∼200 mM (see Figures 5 an 6). At 300, 600, and 1000 μM KCl, the Cs$^+$-induced decreases in T_M are 25 ± 2, 21 ± 2, and 23 ± 2 °C (with an average of 23 ± 1 °C), respectively, while TMA$^+$ ions cause depressions T_M of 15 ± 1, 16 ± 1, and 16 ± 1 °C (with an average of 16 ± 1 °C), respectively.

We have previously observed that nonstabilizing cations exert little to no influence on the thermal stability of human telomeric G-quadruplexes.[40] In the case of the c-MYC promoter sequence, the situation is more dramatic with Cs$^+$ and TMA$^+$ ions exerting strongly destabilizing influence on the G-quadruplex conformation. We rationalize these experimental observations by proposing that the extent of counterion condensation is reduced in the G-quadruplex state of MYC22-G14T/G23T relative to that in the coil state. In other words, there are more counterions (Cs$^+$ or TMA$^+$) associated with the coil state than with the G-quadruplex state. The differential number of thermodynamically dissociated counterions, Δn_{M^+}, for the coil and G-quadruplex states can be estimated from initial slope $(\partial T_M)/(\partial \ln[\mathrm{Cs}^+])$ or $(\partial T_M)/(\partial \ln[\mathrm{TMA}^+])$ in Figures 5 and 6 using eq 3. The estimates yield similar Δn_{M^+} values of −1.1 ± 0.1 and −0.9 ± 0.1 for Cs$^+$ and TMA$^+$, respectively.

The weaker destabilizing effect of TMA$^+$ relative to Cs$^+$ ions may be suggestive of their differential affinity for the G-quadruplex or coil conformation. This possibility is underscored by the fact that TMA$^+$ ions are known to exhibit sequence specificity when binding to DNA duplexes. Specifically, TMA$^+$ ions bind more tightly to AT-rich than to GC-rich duplex DNA, thereby modulating the differential stability of AT- and GC-rich duplexes.[61−64] Further studies are required to assess the notion of the differential affinity of Cs$^+$ and TMA$^+$ ions for the ODN in its G-quadruplex or coil state.

The effect of differential counterion condensation on G-quadruplex stability ceases when the bulk concentration of the counterions approaches their local concentration in the vicinity of the coil state. Thus, the local counterion concentration in the vicinity of the coil state is on the order of ∼200 mM compared to ∼1 M, the estimate for polymeric double-stranded DNA.[30]

Cs$^+$-Induced Unfolding of the K$^+$-Stabilized G-Quadruplex. To the best of our knowledge, the profile shown in Figure 7 is the first reported salt-induced unfolding transition of

a nucleic acid structure. We analyzed the transition within the framework of a two-state approximation in which the fraction unfolded, α, is given by

$$\alpha = K/(1 + K) \tag{4}$$

where $K = K_0(1 + k[\mathrm{Cs}^+])^{\Delta n_{M^+}}$ is the salt-dependent equilibrium constant for the reaction of interconversion between the coil and G-quadruplex states and K_0 is the equilibrium constant in the absence of Cs$^+$ ions.

When the data in Figure 7 are fit with eq 4, the value of K_0 was set to 0.0032, which was estimated from our UV melting data, as $K_0 = \exp(-\Delta G°/RT)$, where $\Delta G° = \Delta H_M(1 - T/T_M)$. For the experimental conditions in Figure 7 (600 μM KCl and 51 °C), the values of T_M, ΔH_M, and $\Delta G°$ are 74.3 ± 0.3 °C, 54.7 ± 1.4 kcal mol^{-1}, and 3.7 ± 1.4 kcal mol^{-1}, respectively. The fit produces a Δn_{M^+} of −1.4 ± 0.1. This value is in good agreement with a value of −1.1, the estimate based on the Cs$^+$ dependence of T_M. The agreement lends credence to our analysis and the two-state approximation used in eq 4.

G-Quadruplexes find a number of promising applications in nucleic acid-based nanodevices as aptamers (the best-known example is the thrombin binding aptamer), cation-dependent and complementary strand-dependent nanoswitches, and molecular beacons.[65] The phenomenon of Cs$^+$-induced unfolding of the MYC22-G14T/G23T G-quadruplex may have implications in developing G-quadruplex-based nano-switch devices. Importantly, in these technological applications, an increase in a cation concentration will result in G-quadruplexes switching to the unfolded (coil) and not the folded state.

Structural Analysis of the Enhanced Stability of the MYC22-G14T/G23T G-Quadruplex. The exceptionally high thermal stability of the MYC22-G14T/G23T G-quadruplex may suggest a weaker inter-phosphate repulsion, a major destabilizing force in nucleic acid structures. The reduction may be caused by structural features and/or neutralization of the negative phosphate charges by the two sequestered potassium ions. These factors, while contributing to the stability of the G-quadruplex, should concomitantly weaken the polyelectrolyte effect. The weakening may also be related to the near-spherical shape of a G-quadruplex that facilitates an increase in the distance between the G-strands and, hence, a decrease in charge density. This possibility is underscored by recent theoretical studies that suggest that a charged spherical construct displays a reduced (but still significant) level of counterion condensation relative to that of a cylinder.[66,67] While these arguments can be put forward with respect to any G-quadruplex, their effect should be stronger in MYC22-G14T/G23T than in, for example, human telomeric G-quadruplexes. The latter exhibit

moderate stabilities, lower affinities for the stabilizing cation, and stronger counterion condensation compared to those of c-MYC.[40,48,49]

The neutralizing influence of the internally bound potassium ions and inter-phosphate repulsion in general should be reflected in the volume, ρ_q, and surface, σ_q, charge densities. Volume charge density, ρ_q, can be evaluated as the ratio of the number of formal charges, N_q, to the molecular volume, V_M, of a G-quadruplex. Surface charge density, σ_q, can be estimated as the ratio of N_q to solvent accessible surface area, S_A. The number of formal charges, N_q, is the number of phosphates minus the number of cations coordinated within the central cavity of the G-quadruplex.

The solvent accessible surface area, S_A, of a G-quadruplex normalized per phosphate can be viewed as a measure of the average inter-phosphate distance, while the molecular volume, V_M, per nucleotide characterizes the compactness of a G-quadruplex and, thus, the average distance between the central ions and the phosphates. Table 1 lists the data on S_A and V_M as well as the volume, ρ_q, and surface, σ_q, charge densities computed for the MYC22-G14T/G23T G-quadruplex along with the telomeric Tel22 and Tel26 G-quadruplexes and "an average" polymeric duplex.[48,49,68] The average volume, ρ_q, and surface, σ_q, charge densities of polymeric duplexes were obtained on the basis of the average solvent accessible surface areas, S_A (162 ± 10 Å^2), and molecular volumes, V_M (281 ± 8 Å^3), of seven polymeric RNA, DNA, and RNA/DNA hybrid duplexes.[68]

Inspection of the data presented in Table 1 reveals that the molecular volume, V_M, of the c-MYC G-quadruplex normalized per nucleotide is 281 ± 1 Å^3. This number is intermediate between those of the Na$^+$-stabilized antiparallel Tel22 (292 ± 1 Å^3) and K$^+$-stabilized hybrid-1 Tel26 (273 ± 1 Å^3) human telomeric G-quadruplexes and coincides with that of polymeric DNA duplexes. Thus, the c-MYC G-quadruplex exhibits an average compactness, being less compact than the Tel26 G-quadruplex but more compact than the Tel22 G-quadruplex. In agreement with this observation, the volume charge density, ρ_q, of the c-MYC G-quadruplex [(3.24 ± 0.01) × 10^{-3} e/Å^3] is intermediate between those exhibited by the Tel22 [(2.96 ± 0.01) × 10^{-3} e/Å^3] and Tel24 [(3.38 ± 0.01) × 10^{-3} e/Å^3] G-quadruplexes, while all being somewhat smaller than that of polymeric duplexes [(3.6 ± 0.1) × 10^{-3} e/Å^3]. Given the intermediate values of molecular volume normalized per nucleotide and volume charge density of the c-MYC G-quadruplex, neutralization of the phosphates by the central ions is, probably, not the main reason for its high thermostability.

The solvent accessible surface area occupied by each phosphate on the surface of the MYC22-G14T/G23T G-quadruplex (202 ± 2 Å^2) is 15−30% larger than that in the Tel22 (178 ± 5 Å^2) and Tel26 (152 ± 3 Å^2) G-quadruplexes or polymeric duplexes (162 ± 10 Å^2). If, as a first approximation, the area assigned to each phosphate is viewed as a square, a 15−30% increase in area translates into a 5−10% larger inter-phosphate distance in the MYC22-G14T/G23T G-quadruplex than in the Tel22 and Tel26 G-quadruplexes. The detected increase in inter-phosphate separation, in turn, signifies weaker charge−charge repulsion and a smaller surface charge density, σ_q, of the MYC22-G14T/G23T G-quadruplex. This notion is consistent with the value of σ_q exhibited by the MYC22-G14T/G23T G-quadruplex [(4.50 ± 0.03) × 10^{-3} e/Å^2] being smaller than those of the two human telomeric G-quadruplexes [(4.9 ±

0.1) × 10^{-3} and (6.1 ± 0.1) × 10^{-3} e/Å^2] and polymeric duplexes [(6.2 ± 0.3) × 10^{-3} e/Å^2] (see Table 1).

In summary, our simplified analysis identifies the structural features of the MYC22-G14T/G23T G-quadruplex resulting in low surface charge density as a possible major contributor to its outstanding thermostability. Given the limited set of analyzed topologies, it is currently unclear if the large inter-phosphate separation is a unique structural characteristics of the MYC22-G14T/G23T G-quadruplex or a general feature of the parallel topology.

As a final note, we cannot exclude the possibility that the hydration properties of the c-MYC G-quadruplex also play a role in rendering it highly stable. This notion stems from the fact that DNA−water interactions, generally, correlate with solvent accessible surface area, S_A, while the MYC22-G14T/G23T G-quadruplex exhibits an unusually large S_A normalized per phosphate. DNA−water interactions represent a crucial determinant of the stability of nucleic acid structure in general and G-quadruplexes in particular.[48,49,69−73] G-Quadruplex-to-coil transitions may greatly vary with respect to the number of water molecules taken up from or released to the bulk, which further underscores the selective role of water in modulating G-quadruplex stability.[48,49,72,73] Clearly, further detailed studies are required to shed light on the balance of molecular forces modulating the stability of G-quadruplexes and the generality of our findings.

■ CONCLUSION

We report a systematic investigation of the thermal stability of a G-quadrupex formed by a modified c-MYC NHE III$_1$ sequence with two G-to-T mutations (5′-TGAGGGTGGGTAGGGTG-GGTAA-3′) in the presence of stabilizing and nonstabilizing cations. Introduction of two G-to-T mutations at residue positions 14 and 23 of the original c-MYC sequence restricts the modified sequence (MYC22-G14T/G23T) to a single, parallel-stranded G-quadruplex conformation. An increase in the concentration of the stabilizing cation K$^+$ causes a steady increase in the melting temperature, T_M, of the MYC22-G14T/G23T G-quadruplex. On the other hand, an increase in the concentration of nonstabilizing Cs$^+$ or TMA$^+$ cations at a constant concentration of K$^+$ ions causes a sharp decline in T_M followed by a leveling off at ~200 mM Cs$^+$ or TMA$^+$. At 51 °C and 600 μM K$^+$, an increase in CsCl concentration from 0 to 800 mM leads to unfolding of the G-quadruplex. These observations are consistent with the picture in which more counterions accumulate in the MYC22-G14T/G23T coil state than in the G-quadruplex state.

Taken together with earlier studies,[40] our data suggest that the stabilizing action of cations originates, primarily, from the sodium or potassium ions sequestered inside the central cavity of a G-quadruplex that act as specifically bound ligands. Nonspecifically bound (condensed) counterions may exert little to no influence (human telomeric G-quadruplexes) or may strongly destabilize (MYC22-G14T/G23T) the G-quadruplex conformation. Our calculations suggest that the very high stability of the MYC22-G14T/G23T G-quadruplex primarily originates from its structural features. In the MYC22-G14T/G23T G-quadruplex, the solvent accessible surface area normalized per phosphate is 15−30% larger than that in human telomeric G-quadruplexes, which translates into a 5−10% greater inter-phosphate distance, lower surface charge density, and, most significantly, weaker charge−charge repulsion. The latter represents a major influence destabilizing

folded nucleic acid structures. In a broader sense, our results underscore the subtle nature of the balance of forces that govern the conformational preferences of biological macromolecules.

■ AUTHOR INFORMATION

Corresponding Author

*E-mail: chalikan@phm.utoronto.ca. Telephone: (416) 946-3715. Fax: (416) 978-8511.

■ REFERENCES

(1) Burge, S., Parkinson, G. N., Hazel, P., Todd, A. K., and Neidle, S. (2006) Quadruplex DNA: Sequence, topology and structure. *Nucleic Acids Res. 34*, 5402−5415.

(2) Huppert, J. L. (2008) Four-stranded nucleic acids: Structure, function and targeting of G-quadruplexes. *Chem. Soc. Rev. 37*, 1375−1384.

(3) Lane, A. N., Chaires, J. B., Gray, R. D., and Trent, J. O. (2008) Stability and kinetics of G-quadruplex structures. *Nucleic Acids Res. 36*, 5482−5515.

(4) Keniry, M. A. (2000) Quadruplex structures in nucleic acids. *Biopolymers 56*, 123−146.

(5) Shafer, R. H., and Smirnov, I. (2000) Biological aspects of DNA/RNA quadruplexes. *Biopolymers 56*, 209−227.

(6) Lam, E. Y., Beraldi, D., Tannahill, D., and Balasubramanian, S. (2013) G-Quadruplex structures are stable and detectable in human genomic DNA. *Nat. Commun. 4*, 1796.

(7) Biffi, G., Tannahill, D., McCafferty, J., and Balasubramanian, S. (2013) Quantitative visualization of DNA G-quadruplex structures in human cells. *Nat. Chem. 5*, 182−186.

(8) Biffi, G., Di, A. M., Tannahill, D., and Balasubramanian, S. (2014) Visualization and selective chemical targeting of RNA G-quadruplex structures in the cytoplasm of human cells. *Nat. Chem. 6*, 75−80.

(9) Rodriguez, R., Miller, K. M., Forment, J. V., Bradshaw, C. R., Nikan, M., Britton, S., Oelschlaegel, T., Xhemalce, B., Balasubramanian, S., and Jackson, S. P. (2012) Small-molecule-induced DNA damage identifies alternative DNA structures in human genes. *Nat. Chem. Biol. 8*, 301−310.

(10) Hurley, L. H. (2002) DNA and its associated processes as targets for cancer therapy. *Nat. Rev. Cancer 2*, 188−200.

(11) Huppert, J. L. (2007) Four-stranded DNA: Cancer, gene regulation and drug development. *Philos. Trans. R. Soc., A 365*, 2969−2984.

(12) Oganesian, L., and Bryan, T. M. (2007) Physiological relevance of telomeric G-quadruplex formation: A potential drug target. *BioEssays 29*, 155−165.

(13) De Cian, A., Lacroix, L., Douarre, C., Temime-Smaali, N., Trentesaux, C., Riou, J. F., and Mergny, J. L. (2008) Targeting telomeres and telomerase. *Biochimie 90*, 131−155.

(14) Oster, S. K., Ho, C. S. W., Soucie, E. L., and Penn, L. Z. (2002) The myc oncogene: MarvelouslY Complex. *Adv. Cancer Res. 84*, 81−154.

(15) Eisenman, R. N. (2001) Deconstructing Myc. *Genes Dev. 15*, 2023−2030.

(16) Wierstra, I., and Alves, J. (2008) The c-myc Promoter: Still MysterY and Challenge. *Adv. Cancer Res. 99*, 113−333.

(17) Gonzalez, V., and Hurley, L. H. (2010) The c-MYC NHE III$_1$: Function and regulation. *Annu. Rev. Pharmacol. Toxicol. 50*, 111−129.

(18) Simonsson, T., Pecinka, P., and Kubista, M. (1998) DNA tetraplex formation in the control region of c-myc. *Nucleic Acids Res. 26*, 1167−1172.

(19) Berberich, S. J., and Postel, E. H. (1995) PuF/NM23-H2/NDPK-B transactivates a human c-myc promoter-CAT gene via a functional nuclease hypersensitive element. *Oncogene 10*, 2343−2347.

(20) Postel, E. H., Berberich, S. J., Rooney, J. W., and Kaetzel, D. M. (2000) Human NM23/nucleoside diphosphate kinase regulates gene expression through DNA binding to nuclease-hypersensitive transcriptional elements. *J. Bioenerg. Biomembr. 32*, 277−284.

(21) Simonsson, T., Pribylova, M., and Vorlickova, M. (2000) A nuclease hypersensitive element in the human c-myc promoter adopts several distinct i-tetraplex structures. *Biochem. Biophys. Res. Commun. 278*, 158−166.

(22) Brooks, T. A., and Hurley, L. H. (2009) The role of supercoiling in transcriptional control of MYC and its importance in molecular therapeutics. *Nat. Rev. Cancer 9*, 849−861.

(23) Sun, D., and Hurley, L. H. (2009) The importance of negative superhelicity in inducing the formation of G-quadruplex and i-motif structures in the c-Myc promoter: Implications for drug targeting and control of gene expression. *J. Med. Chem. 52*, 2863−2874.

(24) Siddiqui-Jain, A., Grand, C. L., Bearss, D. J., and Hurley, L. H. (2002) Direct evidence for a G-quadruplex in a promoter region and its targeting with a small molecule to repress c-MYC transcription. *Proc. Natl. Acad. Sci. U.S.A. 99*, 11593−11598.

(25) Seenisamy, J., Rezler, E. M., Powell, T. J., Tye, D., Gokhale, V., Joshi, C. S., Siddiqui-Jain, A., and Hurley, L. H. (2004) The dynamic character of the G-quadruplex element in the c-MYC promoter and modification by TMPyP4. *J. Am. Chem. Soc. 126*, 8702−8709.

(26) Phan, A. T., Modi, Y. S., and Patel, D. J. (2004) Propeller-type parallel-stranded G-quadruplexes in the human c-myc promoter. *J. Am. Chem. Soc. 126*, 8710−8716.

(27) Ambrus, A., Chen, D., Dai, J. X., Jones, R. A., and Yang, D. Z. (2005) Solution structure of the biologically relevant G-quadruplex element in the human c-MYC promoter. Implications for g-quadruplex stabilization. *Biochemistry 44*, 2048−2058.

(28) Mathad, R. I., Hatzakis, E., Dai, J., and Yang, D. (2011) c-MYC promoter G-quadruplex formed at the 5′-end of NHE III$_1$ element: Insights into biological relevance and parallel-stranded G-quadruplex stability. *Nucleic Acids Res. 39*, 9023−9033.

(29) Chaires, J. B. (2010) Human telomeric G-quadruplex: Thermodynamic and kinetic studies of telomeric quadruplex stability. *FEBS J. 277*, 1098−1106.

(30) Manning, G. S. (1978) Molecular theory of polyelectrolyte solutions with applications to electrostatic properties of polynucleotides. *Q. Rev. Biophys. 11*, 179−246.

(31) Record, M. T., Anderson, C. F., and Lohman, T. M. (1978) Thermodynamic analysis of ion effects on binding and conformational equilibria of proteins and nucleic acids: The roles of ion association or release, screening, and ion effects on water activity. *Q. Rev. Biophys. 11*, 103−178.

(32) Anderson, C. F., and Record, M. T. (1995) Salt-nucleic acid interactions. *Annu. Rev. Phys. Chem. 46*, 657−700.

(33) Anderson, C. F., and Record, M. T. (1982) Polyelectrolyte theories and their applications to DNA. *Annu. Rev. Phys. Chem. 33*, 191−222.

(34) Lipfert, J., Doniach, S., Das, R., and Herschlag, D. (2014) Understanding nucleic acid-ion interactions. *Annu. Rev. Biochem. 83*, 813−841.

(35) Plum, G. E., Pilch, D. S., Singleton, S. F., and Breslauer, K. J. (1995) Nucleic acid hybridization: Triplex stability and energetics. *Annu. Rev. Biophys. Biomol. Struct. 24*, 319−350.

(36) SantaLucia, J., Jr., and Hicks, D. (2004) The thermodynamics of DNA structural motifs. *Annu. Rev. Biophys. Biomol. Struct. 33*, 415−440.

(37) Shkel, I. A., and Record, M. T., Jr. (2004) Effect of the number of nucleic acid oligomer charges on the salt dependence of stability

(ΔG°_{37}) and melting temperature (T_m): NLPB analysis of experimental data. *Biochemistry 43*, 7090−7101.

(38) SantaLucia, J., Jr. (1998) A unified view of polymer, dumbbell, and oligonucleotide DNA nearest-neighbor thermodynamics. *Proc. Natl. Acad. Sci. U.S.A. 95*, 1460−1465.

(39) Tikhomirova, A., Beletskaya, I. V., and Chalikian, T. V. (2006) Stability of DNA duplexes containing GG, CC, AA, and TT mismatches. *Biochemistry 45*, 10563−10571.

(40) Kim, B. G., Shek, Y. L., and Chalikian, T. V. (2013) Polyelectrolyte effects in G-quadruplexes. *Biophys. Chem. 184*, 95−100.

(41) Yang, D. Z., and Hurley, L. H. (2006) Structure of the biologically relevant G-quadruplex in the c-MYC promoter. *Nucleosides, Nucleotides Nucleic Acids 25*, 951−968.

(42) Marky, L. A., and Breslauer, K. J. (1987) Calculating thermodynamic data for transitions of any molecularity from equilibrium melting curves. *Biopolymers 26*, 1601−1620.

(43) Breslauer, K. J. (1995) Extracting thermodynamic data from equilibrium melting curves for oligonucleotide order-disorder transitions. *Methods Enzymol. 259*, 221−242.

(44) Richards, F. M. (1977) Areas, volumes, packing, and protein structure. *Annu. Rev. Biophys. Bioeng. 6*, 151−176.

(45) Richards, F. M. (1985) Calculation of molecular volumes and areas for structures of known geometry. *Methods Enzymol. 115*, 440−464.

(46) Hatzakis, E., Okamoto, K., and Yang, D. (2010) Thermodynamic stability and folding kinetics of the major G-quadruplex and its loop isomers formed in the nuclease hypersensitive element in the human c-Myc promoter: Effect of loops and flanking segments on the stability of parallel-stranded intramolecular G-quadruplexes. *Biochemistry 49*, 9152−9160.

(47) Dapic, V., Abdomerovic, V., Marrington, R., Peberdy, J., Rodger, A., Trent, J. O., and Bates, P. J. (2003) Biophysical and biological properties of quadruplex oligodeoxyribonucleotides. *Nucleic Acids Res. 31*, 2097−2107.

(48) Fan, H. Y., Shek, Y. L., Amiri, A., Dubins, D. N., Heerklotz, H., Macgregor, R. B., and Chalikian, T. V. (2011) Volumetric characterization of sodium-induced G-quadruplex formation. *J. Am. Chem. Soc. 133*, 4518−4526.

(49) Shek, Y. L., Noudeh, G. D., Nazari, M., Heerklotz, H., Abu-Ghazalah, R. M., Dubins, D. N., and Chalikian, T. V. (2014) Folding thermodynamics of the hybrid-1 type intramolecular human telomeric G-quadruplex. *Biopolymers 101*, 216−227.

(50) Rachwal, P. A., and Fox, K. R. (2007) Quadruplex melting. *Methods 43*, 291−301.

(51) Breslauer, K. J. (1994) Extracting thermodynamic data from equilibrium melting curves for oligonucleotide order-disorder transitions. *Methods Mol. Biol. 26*, 347−372.

(52) Buscaglia, R., Gray, R. D., and Chaires, J. B. (2013) Thermodynamic characterization of human telomere quadruplex unfolding. *Biopolymers 99*, 1006−1018.

(53) Breslauer, K. J., Freire, E., and Straume, M. (1992) Calorimetry: A tool for DNA and ligand-DNA studies. *Methods Enzymol. 211*, 533−567.

(54) Privalov, G. P., and Privalov, P. L. (2000) Problems and prospects in microcalorimetry of biological macromolecules. *Methods Enzymol. 323*, 31−62.

(55) Majhi, P. R., Qi, J. Y., Tang, C. F., and Shafer, R. H. (2008) Heat capacity changes associated with guanine quadruplex formation: An isothermal titration calorimetry study. *Biopolymers 89*, 302−309.

(56) Luus, R., and Jaakola, T. H. I. (1973) Optimization by direct search and systematic reduction of size of search region. *AIChE J. 19*, 760−766.

(57) Gray, R. D., Trent, J. O., and Chaires, J. B. (2014) Folding and unfolding pathways of the human telomeric G-quadruplex. *J. Mol. Biol. 426*, 1629−1650.

(58) Bond, J. P., Anderson, C. F., and Record, M. T. (1994) Conformational transitions of duplex and triplex nucleic acid helices: Thermodynamic analysis of effects of salt concentration on stability using preferential interaction coefficients. *Biophys. J. 67*, 825−836.

(59) Cheng, Y. K., and Pettitt, B. M. (1992) Stabilities of double- and triple-strand helical nucleic acids. *Prog. Biophys. Mol. Biol. 58*, 225−257.

(60) Owczarzy, R., Dunietz, I., Behlke, M. A., Klotz, I. M., and Walder, J. A. (2003) Thermodynamic treatment of oligonucleotide duplex-simplex equilibria. *Proc. Natl. Acad. Sci. U.S.A. 100*, 14840−14845.

(61) Shapiro, J. T., Stannard, B. S., and Felsenfeld, G. (1969) The binding of small cations to deoxyribonucleic acid. Nucleotide specificity. *Biochemistry 8*, 3233−3241.

(62) Melchior, W. B., Jr., and von Hippel, P. H. (1973) Alteration of the relative stability of dAdT and dGdC base pairs in DNA. *Proc. Natl. Acad. Sci. U.S.A. 70*, 298−302.

(63) Rees, W. A., Yager, T. D., Korte, J., and von Hippel, P. H. (1993) Betaine can eliminate the base pair composition dependence of DNA melting. *Biochemistry 32*, 137−144.

(64) Portella, G., Germann, M. W., Hud, N. V., and Orozco, M. (2014) MD and NMR analyses of choline and TMA Binding to duplex DNA: On the origins of aberrant sequence-dependent stability by alkyl cations in aqueous and water-free solvents. *J. Am. Chem. Soc. 136*, 3075−3086.

(65) Krishnan, Y., and Simmel, F. C. (2011) Nucleic acid based molecular devices. *Angew. Chem., Int. Ed. 50*, 3124−3156.

(66) Manning, G. S. (2007) Electrostatic free energies of spheres, cylinders, and planes in counterion condensation theory with some applications. *Macromolecules 40*, 8071−8081.

(67) Manning, G. S. (2007) Counterion condensation on charged spheres, cylinders, and planes. *J. Phys. Chem. B 111*, 8554−8559.

(68) Chalikian, T. V., Volker, J., Srinivasan, A. R., Olson, W. K., and Breslauer, K. J. (1999) The hydration of nucleic acid duplexes as assessed by a combination of volumetric and structural techniques. *Biopolymers 50*, 459−471.

(69) Chalikian, T. V., and Volker, J. (2008) Hydration of nucleic acids. In *Wiley Encyclopedia of Chemical Biology* (Begley, T. P., Ed.) John Wiley and Sons, Inc., New York.

(70) Takahashi, S., and Sugimoto, N. (2013) Effect of pressure on the stability of G-quadruplex DNA: Thermodynamics under crowding conditions. *Angew. Chem., Int. Ed. 52*, 13774−13778.

(71) Takahashi, S., and Sugimoto, N. (2013) Effect of pressure on thermal stability of G-quadruplex DNA and double-stranded DNA structures. *Molecules 18*, 13297−13319.

(72) Nakano, S., Miyoshi, D., and Sugimoto, N. (2014) Effects of molecular crowding on the structures, interactions, and functions of nucleic acids. *Chem. Rev. 114*, 2733−2758.

(73) Miyoshi, D., Karimata, H., and Sugimoto, N. (2006) Hydration regulates thermodynamics of G-quadruplex formation under molecular crowding conditions. *J. Am. Chem. Soc. 128*, 7957−7963.

■ NOTE ADDED AFTER ASAP PUBLICATION

This article was published ASAP on May 27, 2015 with incorrect references to the equations due to production error. The corrected version was reposted on May 28, 2015.